Evaluating Binding Avidities of Populations of Heterogeneous Multivalent Ligand-Functionalized Nanoparticles

Ming-Hsin Li,[†,‡] Seok Ki Choi,[‡,§] Pascale R. Leroueil,[‡,§] and James R. Baker, Jr.[†,‡,§,*]

[†]Department of Biomedical Engineering, University of Michigan, Ann Arbor, Michigan 48109, United States, [‡]Michigan Nanotechnology Institute for Medicine and Biological Sciences, University of Michigan, Ann Arbor, Michigan 48109, United States, and [§]Department of Internal Medicine, University of Michigan, Ann Arbor, Michigan 48109, United States

ABSTRACT Ligand-functionalized, multivalent nanoparticles have been extensively studied as targeted carriers in biomedical applications for drug delivery and imaging. The chemical synthesis method used, however, generates nanoparticles that are heterogeneous with respect to the number of ligands on each nanoparticle. This article examines the role this heterogeneity in ligand number plays in multivalent interactions between nanoparticle ligands and targeted receptors. We designed and synthesized a model heterogeneous multivalent nanoparticle system and developed a unique kinetic analysis to quantify the avidity interactions. This system used mono-dispersed poly(amidoamine) (PAMAM) dendrimers that were then chemically functionalized with ssDNA oligonucleotides as to yield the heterogeneous nanoparticle platform (ligand valencies $n = 1.7, 3.1, 6$), and employed complementary oligonucleotides as targeted receptors on a surface plasmon resonance (SPR) biosensor to evaluate the multivalent binding of the nanoparticle population. Kinetic analysis of both parallel initial rate and dual-Langmuir analyses of SPR binding curves was performed to assess avidity distributions. We found that batches of multivalent nanoparticles contain both fast- and slow-dissociation subpopulations, which can be characterized as having "weak" and "strong" surface interactions ("binding"), respectively. Furthermore, we found that the proportion of "strong" binders increased as a function of the mean oligonucleotide valence of the nanoparticle population. These analyses allowed an assessment of how avidity distributions are modulated by the number of functionalized ligands and suggested that there are threshold valences that differentiated fast- and slow-dissociation nanoparticles.

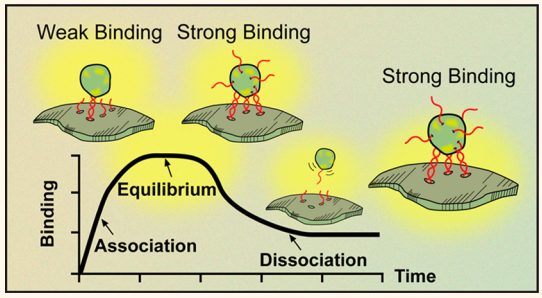

KEYWORDS: avidity · heterogeneity · multivalent binding · oligonucleotide · poly(amidoamine) dendrimer

Much research has focused on developing therapeutics that actively target diseased cells by exploiting the binding specificity of receptors present on their cell surface.[1−3] Active targeting requires highly specific and avid interactions between the therapeutic and the target molecules, to allow the therapeutic to bind and remain bound to the targeted cell surface. Given these requirements, only antibodies and ligand-functionalized, multivalent nanoparticles have proven effective when used as targeted delivery carriers.[4,5] Antibodies have advantages due to their solubility and uniformity; however, low molecular weight ligands of cell receptors, such as vitamins,[6] carbohydrates,[7,8] and drugs,[9,10] are not immunogenic and can bind to targets that are not amenable to antibody production. Many of these ligands with specificity for different types of cells have been identified but their binding affinity is too low to target carried drugs. To overcome these low affinity issues, multiple low-affinity ligands have been attached to the surface of a single nanoparticle, yielding increased binding avidities, circulation times and specific interactions approaching those of antibodies.[11−13]

One confounding factor associated with multivalent interactions involving ligand-functionalized nanoparticles is the heterogeneity of the number of ligands on each particle in the population. In contrast to

* Address correspondence to jbakerjr@med.umich.edu.

Received for review December 17, 2013 and accepted May 8, 2014.

Published online May 08, 2014
10.1021/nn406455s

antibodies, multivalent nanoparticles by nature of their chemical synthesis are a heterogeneous population of macromolecules with distributed numbers of ligands. When characterized by typical analytical techniques, such as NMR, UV−vis, mass spectrometry (MS), and gel permeation chromatography (GPC), the measured number of ligands per nanoparticle represents an *average* number that does not fully describe the heterogeneity of the population distribution.[14−16] The extent of this heterogeneity was recently revealed by extensive analyses of a variety of functionalized nanoparticles using both theoretical calculations and exacting experimental analysis.[17,18] This work demonstrated that the number of functionalized ligands per particle is often highly variable, leading to a concern this could result in heterogeneous ligand−receptor interactions and distributed binding avidities with targeted cell surfaces. Even if the average number of ligands seems to be sufficient to support multivalent interactions, this heterogeneity makes it likely that a subpopulation of less-functionalized nanoparticles would not effectively target cells-surface receptors. More importantly, if these low-affinity nanoparticles carried toxic drugs or heavy-metal contrast agents *in vivo*, these subpopulations could lead to variable therapeutic effects due to prolonged circulation times without retention within targeted tissues. Therefore, a technique that can determine whether populations of nanoparticles can achieve multivalent avidities adequate to target cells would be important to develop ligand-functionalized nanoparticles and optimize ligand design.

Unfortunately, techniques to characterize the effectiveness of nanoparticles with different valencies currently do not exist. The most relevant analysis uses affinity chromatography to separate the heterogeneous nanoparticle populations and assess their ligand number.[5] This approach does not provide adequate material to directly assess the avidity of these subpopulations and cannot examine the binding of the population as a whole when high and low ligand substituted nanoparticles compete with one another. In this article, we present a method that can quantitatively evaluate the heterogeneous avidities presented by ligand-functionalized nanoparticles. This method involves a surface plasmon resonance (SPR) biosensor to analyze multivalent interactions of a well-controlled model system composed of monodisperse poly(amidoamine) (PAMAM) dendrimers as the nanoparticles and complementary ssDNA oligonucleotides as the ligands and targeted molecules. This binding system was chosen due to the ease of designing and synthesizing ssDNA oligos with specific and varied sequences that result in varied binding affinities.[19] In addition, oligonucleotide ligands have proven useful in designing novel biomedical platforms and for drug delivery and devices.[20,21] Using SPR, we demonstrated that a heterogeneous

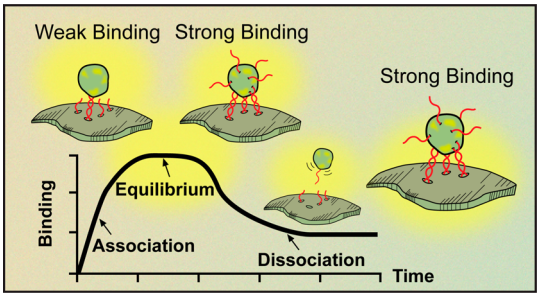

Figure 1. Kinetic analysis of both parallel initial rate and dual-Langmuir analyses of SPR binding curves was performed to assess avidity distributions. We found that batches of multivalent nanoparticles contain both fast- and slow-dissociation subpopulations, which can be characterized as having "weak" and "strong" surface interactions ("binding"), respectively.

population of ligand-functionalized nanoparticles showed two discrete types of binding: a weak and a strong component. From these data, we were able to develop a unique kinetic analysis to quantify the subpopulations responsible for the avidity distributions. Importantly, these results indicate that in these heterogeneous populations only a small portion of ligand-functionalized nanoparticles gain significant avidity enhancement due to their multivalent structure, as depicted in Figure 1. Using this method to examine nanoparticle populations with varied average valencies, we demonstrate that the avidity distribution of synthetic multivalent nanoparticles is determined by the valency distribution of the functionalized ligands. Comparing the results of a Poisson simulation of distributed ligands on nanoparticles and their resulting avidity distribution, we further suggest that there is a cutoff valence required to initiate multivalent interactions. This "threshold valence" could be a factor broadly applied to the design of multivalent nanoparticle systems.

RESULTS AND DISCUSSION

Design and Synthesis of PAMAM Dendrimer-Based Multivalent Nanoparticles. To develop a practical understanding of targeting parameters with ligand-functionalized multivalent-targeted nanoparticles, it was important to develop a system where the molecules could be well-defined and controlled for different parameters that could alter binding kinetics. In this report, we employed 8-mer ssDNA oligonucleotides (oligos) as ligands with corresponding complementary oligonucleotides as the targets, coupled to G5 PAMAM dendrimers as the nanoparticles. We focused on 8-mer ssDNA oligos in this study because it approximates the size of most small molecule targeting ligands and we could design a sequence demonstrating micromolar affinity (K_D) for a complementary oligo comparable to the binding affinity of most small molecule ligands.[22,23] G5 PAMAM dendrimer as nanoparticles also aids our investigations due to its monodispersity, biocompatibility, and water-solubility.[24,25] Importantly, its abundant

Scheme 1. Synthesis of oligonucleotide-functionalized G5 PAMAM dendrimers functionalized with oligos *via* an amide-bond ligation.[a,b]

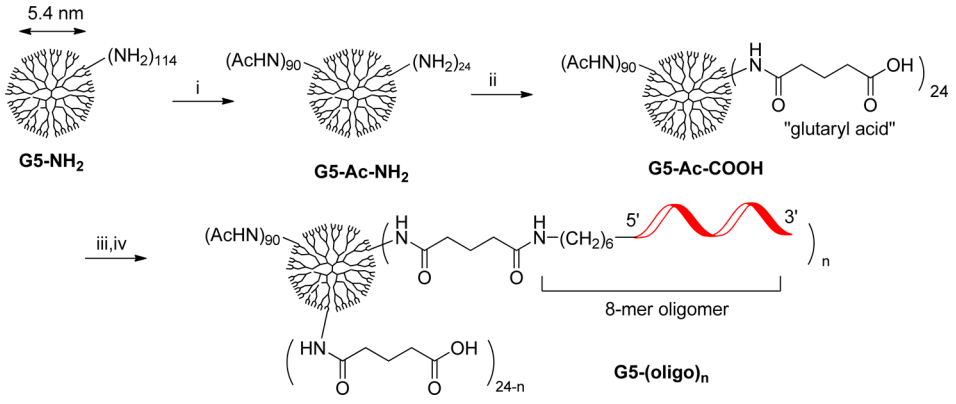

[a] Reagents and conditions: (i) acetic anhydride, triethylamine, MeOH, rt, 16 h; (ii) glutaric anhydride, triethylamine, DMSO, rt, 16 h; (iii) EDC, NHS, DMSO, rt, 2 h; (iv) variable equiv of 8-mer amine-terminated oligonucleotide (5′-H_2N-$(CH_2)_6$-TGCTGAGG), pH 9 carbonate buffer, rt, 16 h. Each of G5-$(oligo)_n$ (n = 6.0, 3.1, and 1.7) was synthesized by reaction with 20, 10, and 5 equiv of oligonucleotides (5′-TGCTGAGG), respectively. [b] G5-NH_2 and its modified dendrimers were fully characterized as described in the Methods section. In particular, number of amine, acid, or oligomer per dendrimer was determined on a mean basis: G5-$(NH_2)_{114}$ and G5-Ac-$(NH_2)_{24}$ (potentiometric titration), G5-Ac-$(COOH)_{24}$ (^{1}H NMR), G5-$(oligo)_n$ (UV−vis).

primary amine surface aids in the approach to synthesizing multivalent nanoparticle systems.

The synthetic approach for the ssDNA oligo-functionalized multivalent nanoparticles is shown in Scheme 1. The functionalization of amine-terminated G5 PAMAM dendrimers (G5-NH_2) initially involved serial reactions of partial acetylation and carboxylation, giving the dendrimer a bifunctional surface. This predominantly neutral surface was tailored to both preserve the ligand amide-bond coupling chemistry yet reduce nonspecific, charge based interactions due to residual protonated primary amines. Subsequent to the surface modification, the coupling reaction between the carboxylic groups on dendrimers and the amine-terminated ssDNA oligos was carried out using 1-ethyl-3-(3-dimethylaminopropyl-)carbodiimide (EDC) and *N*-hydroxysuccinimide (NHS) catalyzed chemistry. With 80% acetylated and 20% carboxylic functional groups on the surface, the G5 PAMAM dendrimers (G5-Ac-COOH) were reacted with 20 equiv of amino-terminated ssDNA oligos, and this resulted in an average of six covalently linked ssDNA oligos on the dendrimer, based on the results of UV−vis spectroscopy at OD_{260}. Also, conjugation was carried out with 5 and 10 equiv of oligos, yielding G5-$(oligo)_{1.7}$ and G5-$(oligo)_{3.1}$, respectively. This indicated an overall reaction yield of approximately 30% for this EDC/NHS coupling reaction. Increasing the carboxylic groups on the dendrimer surface did not improve the efficiency of conjugation and very high degrees of surface carboxylation actually decreased the reaction yield suggesting surface interference.

SPR Measurement of Synthetic Multivalent Nanoparticles. The interaction of ssDNA oligo-functionalized multivalent nanoparticles G5-$(oligo)_6$ and complementary ssDNA oligos was measured using an SPR biosensor. The streptavidin-precoated SPR sensor chip was immobilized with biotin-terminated (5′ end) 25-mer ssDNA oligos that included an internal segment with 8 nucleotides complementary to the 8-mer ssDNA oligo on the dendrimer, while the rest of the oligonucleotide served as a linker. During SPR measurements, G5-$(oligo)_6$ showed enhanced binding as compared to that observed with free oligonucleotides at the same molar concentration. The binding curves of G5-$(oligo)_6$ featured remarkably slow dissociation as compared to the relatively rapid dissociation of free 8 mer ssDNA oligos (Figure 2). After only 2 min of association followed by a 5 min dissociation phase, more than one-third of the surface-bound nanoparticles were still stably adhered to the complementary surface, whereas the free oligonucleotides were completely removed under these conditions. In addition, we found an unusual phenomenon; the SPR association curves of the multivalent nanoparticle did not reach equilibrium after 2 min of association but continued to show gradual increases in surface binding. To understand this unusual binding curve, we conducted a series of SPR tests where we varied the association time in order to compare the equilibrated binding of the nanoparticles (Figure 3). Surprisingly, none of these binding curves plateaued as expected, even when the association time was allowed to approach the limitations of the instrument. This "non-equilibrated" binding strongly suggests there were near "irreversible" interactions taking place on the sensor chip surface. The binding could still be prevented by a prior exposure of the surface to free complementary but not scrambled oligonucleotides (without the surface being washed),

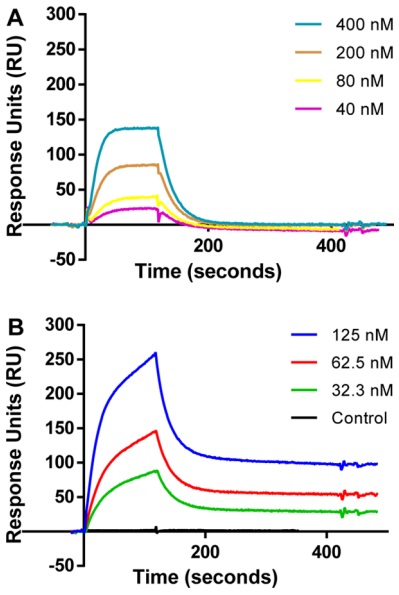

Figure 2. SPR binding curves of different concentrations of free oligonucleotide ligands. (A) Free oligonucleotides at concentrations of 400, 200, 80, and 40 nM were allowed to interact with complementary oligonucleotides fixed to the surface. The duration of the association and dissociation phases is 2 and 5 min, respectively. Note the free oligonucleotides are completely washed off the surface under the conditions of the disassociation phase. (B) Binding curves of oligonucleotide–dendrimer conjugates [G5-(oligo)$_6$] with an average of 6 oligonucleotides per dendrimer (identical oligonucleotides to those in panel A). Dendrimer conjugates are evaluated under identical conditions at oligonucleotide concentrations of 32.3, 62.5, and 125 nM. Control dendrimer [G5-Ac-COOH] was measured at a concentration of 62.5 μM. Note that in contrast to panel A, not all the material is removed from the surface during the disassociation phase.

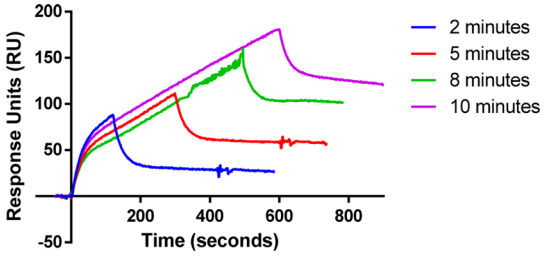

Figure 3. SPR binding curves of G5-(oligo)$_6$ with varied durations of the association phase. The association times are 2 (blue), 5 (red), 8 (green), and 10 min (purple), followed by 5 min of dissociation. The oligonucleotide concentration of G5-(oligo)$_6$ was 62.5 nM.

showing the specificity of the interaction (data not shown).

The series of binding curves produced with varying increases in association time were all consistent with an initial sharp increase in binding followed by a transition showing a clear inflection point, after which there was a slower and linear increase in binding. We also found that the first phase of accumulation of bound nanoparticles and the timing of the transition point were similar among different populations of particles with varied ligand number. In contrast, the

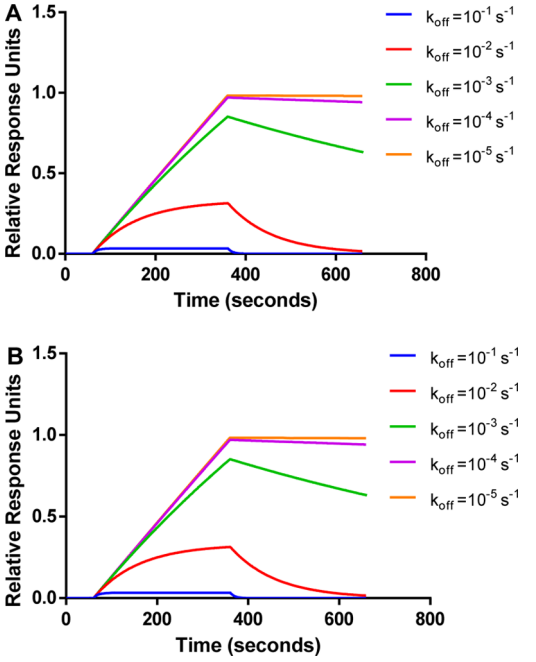

Figure 4. Simulated SPR binding curves of ligands with varied kinetic parameters using 1:1 Langmuir kinetic model. The dissociation constants (k_{off}) include 10^{-1}(blue), 10^{-2} (red), 10^{-3} (green), 10^{-4} (purple), and 10^{-5} (orange) (s^{-1}). (A) $k_{on} = 10^3$ and (B) $k_{on} = 10^5$ (M^{-1} s^{-1}). The concentration of ligand is 62.5 nM. The duration of association and dissociation is 5 min. The units are relative response units (RU/RU$_{max}$).

accumulation of bound nanoparticles after the inflection point was varied between the populations of nanoparticles and related to the mean number of ligands. From this data it was clear that multivalent nanoparticles demonstrated two distinguishable binding behaviors; a subpopulation with apparent weaker binding nanoparticles that would reach equilibrium of binding at a transition point and a second subpopulation demonstrating nearly irreversible binding suggestive of a stronger avidity interaction.

This secondary population also demonstrates a linear increase during the association phase that is characteristic of strong binding. On the basis of a simulation using the Langmuir kinetic model, the dissociation rate constant (k_{off}) of this population should be lower than 10^{-3} s^{-1}, which is significantly slower than the k_{off} of the identical free ssDNA oligo (>10^{-1} s^{-1}), and predicts a straight association curve (Figure 4). Thus, while the result was unusual given the nonlinear association curves that have been generated with some other multivalent nanoparticles, and kinetic models predict this nonequilibrated linear binding.

In addition to the binary behavior seen during the association of the nanoparticles to the sensor, two-phase activity was also observed during the dissociation phase. Regardless of the association time, the dissociation curves displayed similar patterns that initially show a fast dissociation followed by an extremely

slow dissociation phase. The duration and the number of nanoparticles dissociated from the surface during the fast dissociation phase were identical among varied binding curves (Figure 3) strongly suggesting a subpopulation with weaker binding. In contrast, the nanoparticles that remain bound to the surface after the fast dissociation increased approximately linearly with the duration of the sample injections, suggesting a smaller subpopulation with nearly irreversible binding. Taken together, both the association and the dissociation phases of this heterogeneous multivalent nanoparticle system suggest the existence of two subpopulations of nanoparticles: a major population showing weak binding with a rapid binding equilibrium and fast dissociation and a smaller population demonstrating a strong interaction with minimal dissociation. This may be solely the result of secondary binding events, which occur more commonly with particles having higher numbers of ligands. However, it may also be because the initial interaction of the complementary DNA strand on the surface and the particle is more likely to involve all 8 nucleic acids bound to their cognate in particles bearing multiple oligonucleotides. This would provide two reasons for stronger binding with increasing ligand number.

Characterizing the Distribution of Multivalent Nanoparticles That Results in Binary Binding Phases. The first step in characterizing the subpopulations of nanoparticles that result in the binary avidity distribution was to quantify the molar fractions of the subpopulations. This involved a parallel, initial-rate kinetic analysis that included directly measuring the initial rate for the entire population and extrapolating an initial rate for the subpopulation with enhanced avidity. The measured initial rate was readily determined directly from the SPR sensograms, as described previously.[26] This allowed us to derive an equation representing the initial rate analysis (presented as eq 1) where R represents the measured response unit (RU), which is proportional to the mass density of molecules bound to the chip surface. Additionally, R_{max} is the maximum capacity of the RU of the immobilized receptor and C stands for the overall concentration of particles. This equation is derived from the 1:1 Langmuir binding kinetic eq 2 where the change of RU is determined by both the association and dissociation terms (The detailed mathematical derivation of these equations is described in the Supporting Information). The fact that in the initial binding process there are no prebound ligands allows one to neglect the R value in order to derive eq 1.

Evaluating the Subpopulation of Slow-Dissociation Nanoparticles To Derive the Initial Rate Equation for Them. Although it is impossible to directly measure the initial rate for this subpopulation, we can assume that the initial rate is comparable to the rate associated with the linear binding segment located after the inflection, as discussed previously. The equation of the extrapolated initial rate analysis is presented as eq 3, where R_s and C_s stand for the RU and the concentration of particles showing slow dissociation, respectively, and the extrapolated initial rate, dR_s/dt, was extracted by using the average dR/dt after an association time at 2 min.

On the basis of eqs 1 and 3, the fraction of the enhanced-avidity subpopulation, C_s/C, was extracted by using the ratio of dR_s/dt and dR/dt.

$$\left.\frac{dR}{dt}\right|_0 = R_{max} \times k_{on} \times C \quad (1)$$

$$\frac{dR}{dt} = k_{on} \times C \times (R_{max} - R) - k_{off} \times R \quad (2)$$

$$\left.\frac{dR}{dt}\right|_0 = R_{max} \times k_{on} \times C_s \quad (3)$$

On the basis of the parallel initial rate analysis described above, the binary composition of G5-(oligo)$_6$ was evaluated (Figure 5). The directly measured initial rate, $(dR/dt)|_0$, and the extrapolated initial rate, $(dR_s/dt)|_0$, were extracted, and were 2.18 and 0.217 (RU/s), respectively. Given the ratio of these two rates,

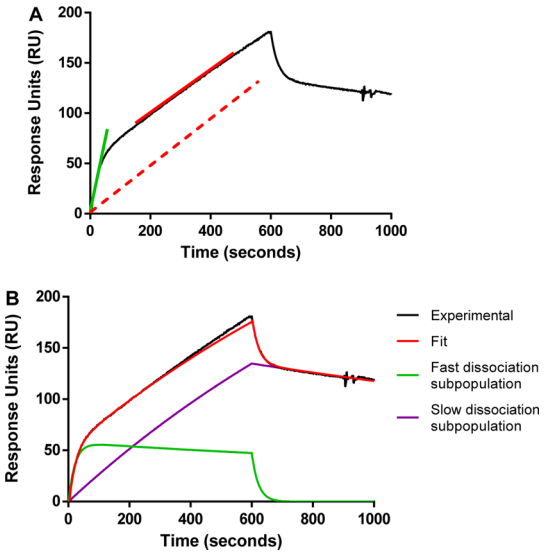

Figure 5. Avidity distribution of G5-(oligo)$_6$ was determined by parallel initial rate analysis (C_s:C = dR_s/dt:dR/dt) and dual Langmuir kinetic analysis. (A) The Initial rate of the entire population (dR/dt) and slow-dissociation subpopulation (dR_s/dt) was extracted using the first derivative of initial binding curve (green) and second phase of association (red solid line), which extrapolated the "real" initial rate of the slow-dissociation subpopulation (red breaking line). (B) When we use concentrations extracted with parallel initial rate analysis, the binding curve can be accurately interpreted using dual Langmuir kinetic model. The experimental binding curve (black) and the fitted binding curve of G5-(oligo)$_6$ (red) showed highly significant relevance (χ^2 = 0.76). The hypothesis that G5-(oligo)$_6$ could demonstrate equilibrated and nearly equilibrated binding was validated by the fitted binding curves of the two subpopulations in G5-(oligo)$_6$ including fast-dissociation subpopulation (green) and slow-dissociation subpopulation (purple).

approximately 10% of the G5-(oligo)$_6$ population showed strong binding. This result provides evidence to support the hypothesis that in these heterogeneous materials, only a small proportion of ligand-functionalized nanoparticles would lead to strong interactions suggestive of avidity interactions. The fact that the high avidity-displaying nanoparticles are a minor portion also indicates that synthesis or design of this multivalent particle requires further improvement for use in targeting.

The parallel initial rate analysis is a valid approach to evaluate these populations with certain assumptions including (1) that variations in the association rate constant, k_{on}, within the nanoparticle system are negligible; that is, the strength of avidity for multivalent nanoparticles is actually determined by their dissociation rates and (2) that the slope of association in the linearly increasing region can be regarded as the initial rate of association of the high affinity nanoparticles, that is $(dR_s/dt)|_0 \approx (dR_s/dt)_{t>ti}$, where ti stands for the inflection point of the binding curve. Fortunately, these assumptions have been validated in several ways. Prior studies with heterogeneous, ligand-functionalized nanoparticles have demonstrated that even with significantly different K_D these particles show an insignificant variation of the association rate constant, k_{on}.[23] Additionally, a simulation method using Langmuir kinetic analysis to conduct a systematic survey of kinetic curves featuring a broad range of the association and dissociation rate constants reinforced the credibility of these proposals (Figure 4). By using the dR/dt of the linear segment of the association curve as the initial rate, the deviation between the extrapolated and real initial rates was less than 5%. This assessment was based on the simulation result with k_{off} at 10^{-3} s^{-1}. The simulation also predicts the deviation between two initial rates would decrease with the k_{off} of the binding, indicating that, when considering the high-avidity component, it is accurate to use the extrapolated initial rate in a parallel initial rate analysis. Because the G5-(oligo)$_6$ showed stable and linear increases during associations, suggesting the k_{off} is smaller than 10^{-3} s^{-1}, the method of parallel rate initial analysis is valid for this system.

Once the composition of nanoparticle subpopulations is quantified a kinetic model can be used to interpret the binary interaction of the multivalent nanoparticle system. Using a dual-Langmuir kinetic analysis, the kinetic parameters of interaction presented by the G5-(oligo)$_6$ were determined. (Table 1). This two-component model generated a curve that closely resembled the curve that was generated experimentally. Furthermore, the chi square value, χ^2, was 4-fold less than the criterion of a solid fit and mathematically reinforced that the nanoparticles interacted with the complementary surface as a binary system.[22] In contrast, when using a simpler 1:1 Langmuir kinetic model to analyze the interaction of these nanoparticles, the fitted curve markedly deviated from the measured reading and the χ^2 was larger than 300. This is 100-fold larger than the acceptable χ^2 of a nonlinear regression, indicating that this synthetic nanoparticle system could not be represented by a single mode of interaction.

TABLE 1. Avidity Distribution and Kinetic Parameters of Oligonucleotide-Functionalized Nanoparticles

nanoparticles	Fr, %	k_{on} (M^{-1} s^{-1})	k_{off} (s^{-1})	K_D (M)
G5-(oligo)$_6$	10	3.10×10^4	3.37×10^{-4}	1.09×10^{-8}
	90	3.31×10^4	4.61×10^{-2}	1.39×10^{-6}
G5-(oligo)$_{3.1}$	<1	3.71×10^3	3.44×10^{-4}	9.26×10^{-8}
	>99	3.57×10^3	3.74×10^{-2}	1.05×10^{-5}

The kinetic parameters of both the fast- and slow-dissociation nanoparticle populations, including k_{on}, k_{off}, and K_D, were individually evaluated. On the basis of the results of the kinetic analysis, approximately a 2-order-of-magnitude enhancement of binding avidity was obtained for the slow-dissociation G5-(oligo)$_6$ with an avidity of approximately 10 nM. In contrast, the fast-dissociation nanoparticles produced an "avidity" of about 1 μM, which is similar to the affinity of the free ssDNA oligonucleotides. Thus, the kinetic information offers a quantitative approach to determine the avidity distribution of synthetic multivalent nanoparticles, which is not achieved by using typical Langmuir kinetic analysis.

Using this approach, we found that the "monovalent-like" interaction demonstrated by the low affinity nanoparticle population showed insignificant avidity enhancement while the "multivalent" interaction of the slow-dissociation nanoparticles showed a 100-fold enhancement. Additionally, the findings that the nanoparticles fall into two discrete populations based on their avidity suggests that multivalent avidity enhancements may result from "step-wise" increases rather than a continuous improvement. Higher avidity interactions may be difficult to obtain as shown by the example of the G5-(oligo)6 system where 90% of the nanoparticles had monovalent-like interaction, despite the fact that 98% of the nanoparticles had more than one ligand. This suggested that there is a significant "energy threshold", perhaps governed by the orientation and location of the ligands, required to activate the multivalent interactions; this was further reinforced by the absence of "in-between" avidity interactions in this system. Taken together, this binary binding avidity suggests that the multiple oligonucleotides on a nanoparticle would not guarantee that multivalent interactions occur.

Evaluating the Effect of Valence on Avidity Populations of Multivalent Nanoparticles. Investigations into multivalent-targeted nanoparticles have studied the role of ligand valence of a nanoparticle on enhancement of binding avidities.[22] However, a major limitation of this work is

that the particles were evaluated as a homogeneous system representing an average binding avidity, which did not dissect the actual interaction of the populations within these complex ligand–nanoparticle systems. Our kinetic analysis allows a specific evaluation of the effect of valence on the avidity interaction of nanoparticles. We evaluated the interaction of two additional populations of nanoparticles that were synthesized with identical oligonucleotide ligands and chemistry, but with an average of either 1.7 or 3.1 ligands per particle [G5-$(oligo)_{1.7}$ and G5-$(oligo)_{3.1}$ respectively]. When the binding of these particles to the same, complementary oligonucleotides on the SPR biosensor surface was evaluated (Figure 6), only the G5-$(oligo)_{3.1}$ demonstrated a biphasic binding component similar to the G5-$(oligo)_6$, including a slow dissociation population indicative of enhanced avidity. In contrast, the G5-$(oligo)_{1.7}$ material reached a binding equilibrium early in the association phase and then rapidly dissociated from the surface, similar to the weak binding component of the G5-$(oligo)_6$ and free ssDNA oligo. We believe the G5-$(oligo)_{1.7}$ material did have a Poisson distribution of ligands on the particles but failed to demonstrate a multivalent population because there were too few nanoparticles with sufficient ligand valence to measure this type of binding.

On the basis of the parallel initial rate analysis and dual Langmuir analysis, the avidity distribution and kinetic parameters of G5-$(oligo)_{3.1}$ were further quantitated (Table 1). Fewer than 1% of slow-dissociation nanoparticles were present in the G5-$(oligo)_{3.1}$, which was 10-fold lower than the amount of this subpopulation present in the G5-$(oligo)_6$. The finding that a 2-fold lower average ligand valence leads to 10-fold decrease of slow-dissociation nanoparticles revealed how sensitive this interaction is to valence and suggests that when the required valence is not attained, avidity enhancement is not achieved.

Although altering the mean ligand valence significantly changed the proportion of strong binding nanoparticles, the nanoparticles present had almost identical kinetic parameters; the weak binding avidity population was always comparable to the affinity of a monovalent ligand interaction while the strong binding population consistently gained a 2-order-of-magnitude avidity improvement. We believe that similarity in kinetics resulted from similar ligands and particles used to develop these populations but essentially were determined by the number of functionalized ligands on nanoparticles; in other words, the strong binding populations had similar numbers of ligands, but there were just fewer of these particles resulting from the synthesis. Other support for this concept comes from recent studies that have showed the ligand-to-nanoparticle ratio in these types of syntheses is heterogeneous and Poisson-distributed.[17] Therefore, we hypothesize that the quantity of strong-binding nanoparticles is determined by the percentage of functionalized nanoparticles that have exceeded the number of ligands per dendrimer required to initiate a multivalent interaction.

We attempted to validate this hypothesis by examining the relationship between the avidity and ligand distributions in these oligonucleotide-functionalized multivalent nanoparticles. Based on the assumption that the multivalent effect is positively associated with the valence, we correlated the Poisson ligand distribution and the avidity distribution of the G5-$(oligo)_6$, and suggest that the 10% of the nanoparticles showing enhanced binding avidity are likely those particles presenting more than 9 ligands (Figure 7). When we then used this valence as a cutoff value, we also observed that in the G5-$(oligo)_{3.1}$ there were 10% fewer and in the G5-$(oligo)_{1.7}$ there were no nanoparticles showing a valence higher than 9; this correlated well with the experimental results. This offers quantitative evidence that the avidity distribution observed in our studies is mediated by the ligand distribution on the nanoparticles. Furthermore, it suggests that increasing the average ligand per nanoparticle increases the proportion of conjugates in the heterogeneous population that are above the threshold valence. This is despite the Poisson variation in ligand number inherent in these particle populations.

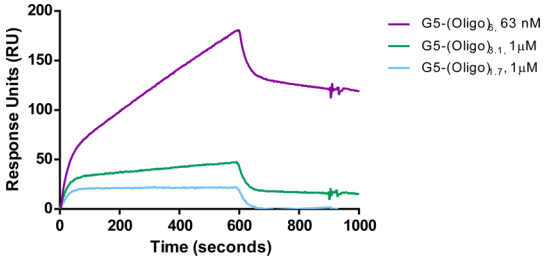

Figure 6. SPR sensograms of three different oligonucleotide-functionalized nanoparticles binding to a complementary oligo functionalized SPR surface. G5-$(oligo)_6$ at 62.5 nM (purple), G5-$(oligo)_{3.1}$ at 1 μM (green), and (iii) G5-$(oligo)_{1.7}$ at 1 μM (light blue) were evaluated at the same amount of total ligand. The durations of the association and dissociation phases are 10 and 5 min, respectively.

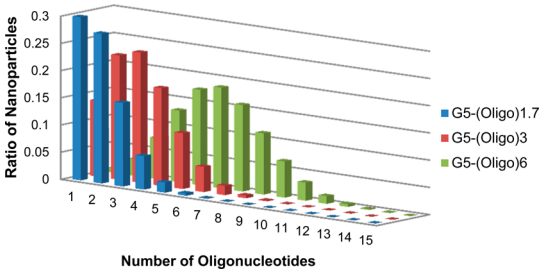

Figure 7. Poisson simulations of the ligand distributions for the three populations of oligonucleotide-functionalized nanoparticles. G5-$(oligo)_{1.7}$ (blue), G5-$(oligo)_{3.1}$ (red), and G5-$(oligo)_6$ (green) show a marked variation between the mean and median number of ligands per dendrimer.

Previous studies have tried to employ high valences in order to maximize the binding avidities in ligand-functionalized nanoparticles.[27−29] Although these studies successfully increased the binding avidities of nanoparticle populations, the binding patterns of these heterogeneous systems uniformly showed binding characterized by bimodal dissociation. This has often been overlooked, and while these results "qualitatively" demonstrated heterogeneous binding avidities, the exact avidity distribution requires "quantitative" evaluation. Re-examining these studies using kinetic analyses could be particularly useful to provide this type of information. While we believe that in different ligand-functionalized nanoparticle systems the threshold valence could be significantly different depending on characteristics of the ligands and nanoparticles, our approach should be universally applicable to analyzing these populations.

Implications of These Findings for Multivalent Nanoparticles as a Targeted Delivery System. In addition to providing comprehensive information about the binding kinetics of synthetic multivalent nanoparticles, our analyses are informative with respect to real-world biopharmaceutical development. While these studies were completed using complementary oligonucleotides as the ligand−receptor pair, the theoretical framework generated from this work can be applied to all types of ligand−receptor pairs. Indeed, the only input required for the analyses is SPR binding curves for a series of conjugates with known averages of ligands per nanoparticle. Even without explicit knowledge of a ligand−receptor pair, these techniques can rapidly evaluate the targeting potential of ligand-functionalized nanoparticles by assessing the avidity distribution. Since it is likely that only multivalent ligands showing stable surface binding in SPR will be able to achieve targeting *in vivo* where particles are under shear from pulsatile blood flow, we believe identifying the percentage of enhanced-avidity nanoparticles would be a practical indicator of the drug targeting potential of those macromolecules. The simulation using the two-component Langmuir kinetic model further supports this concept and suggests that the fraction of slow-dissociation nanoparticles determined the number of nanoparticles attached to the receptor surface. On the basis of this analysis, 2- to 3-fold increase in slow-dissociation nanoparticles could lead to doubled and tripled cell-specific binding (Figure 8). Thus, simply identifying the threshold valence and quantifying this population would be an efficient method to assess the targeting potential before the need to extract kinetic parameters.

Moreover, using a parallel initial rate analysis as we did with our model system can provide the percentage of enhanced-avidity nanoparticles in real time without requiring substantial postprocessing of the material (such as purification of the subpopulations using affinity chromatography) and without complex numerical or mathematical transformations. Although the initial rate analysis originated from the solutions of ordinary differential equations, the acquisition of this fraction is achieved using a graphical method involving two slopes of a kinetic binding curve in a series. One can efficiently extract the fraction of slow-dissociation (targeting-potential) nanoparticles simply from the observation of the SPR-measured kinetic curve without requiring an accurate first-order derivative. Our results suggest this easily obtained parameter would be valuable in SPR-based high-throughput screening of multivalent nanoparticles developed for biomedical targeting applications. The results also infer that it might be feasible to enhance the size of the population of high avidity particles if one could increase the percentage of particles with higher numbers of ligands, potentially through more efficient chemistry.

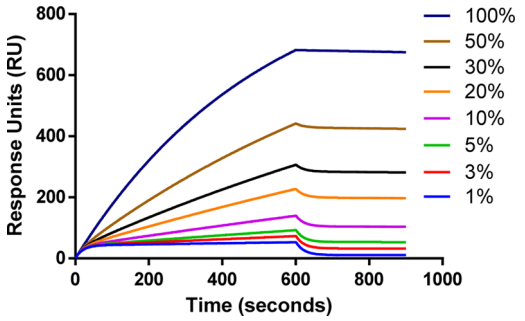

Figure 8. Simulated binding curves of ligands with varied avidity distribution as determined by the dual Langmuir kinetic model. The concentration is 62.5 nM and kinetic parameters of G5-(oligo)$_6$ served as k_{off} and k_{on} in this simulation. The percentages of slow-dissociation subpopulation are 1 (blue), 3 (red), 5 (green), 10 (purple), 20 (cyan), 30 (orange), 50 (dark blue), 100 (dark red) %. The durations of association and dissociation are 10 and 5 min, respectively.

CONCLUSIONS

These studies clarify the structure−function relationship that promotes multivalent ligand−receptor interactions in nanoparticle systems. While ligand-functionalized nanoparticles are usually defined as homogeneous systems with a specific number of ligands, the chemistry involved in conjugating these materials results in heterogeneous systems that present distributed numbers of functionalized ligands. To evaluate the discrete binding activities of these subpopulations, we first developed a model system that allowed the definition of the parameters involved in multivalent interactions and provided the basis to perform kinetic analyses that identify ligand defined nanoparticle subpopulations. In these studies, we demonstrate that only a small portion of ligand-functionalized nanoparticles actually have binding enhancement suggestive of avidity and we evaluated the effect of varied mean ligand number on the avidity distribution of the multivalent nanoparticles. This showed that the impact of average valence is more significant to the molar

fractions of nanoparticles showing avidity binding than it is on the quantitative enhancement of the binding avidities. Comparing the results of Poisson simulations demonstrating "structural" distribution of nanoparticle ligands and the experimentally derived binding "functional" data, we validated a threshold valence required to initiate multivalent interactions and showed its potential to provide a quantitative approach to predict and optimize the binding avidity of multivalent nanoparticles. This suggests one could develop multivalent nanoparticles with homogeneously strong binding avidity by ensuring each nanoparticle has a ligand number surpassing the threshold valence required for multivalent binding. Moreover, this unique analytical method could offer predictive kinetics in a real-time fashion that would be valuable in high-throughput approaches for developing discrete targeting ligand systems on nanoparticles.

METHODS

Chemicals and Materials. Single-stranded DNA oligonucleotides (ssDNA oligos) were synthesized with 5′-end modifications and purified with a standard desalting process at Integrated DNA Technologies (Coralville, IA), including an 8-mer amino-terminated oligo, 5′-NH_2-C_6-TGCTGAGG, and a 25-mer biotinylated oligo 5′-biotin-TTTCCTCAGCATCTTATCCGAGTTTT. The generation 5 poly(amidoamine) (G5 PAMAM) dendrimer was purchased from Dendritech, Inc. (Midland, MI) and was purified as described in the synthesis section. All organic solvents, reagents, and titration volumetric solutions (0.1 M HCl and 0.1 M NaOH) were purchased from Sigma-Aldrich (St. Louis, MO) and used without further purification. Phosphate buffer saline (PBS) without calcium and magnesium was purchased from Thermo Scientific (Logan, UT). The 10K molecular weight cutoff (MWCO) centrifugal filters (Amicon Ultra-4) were purchased from Millipore (Billerica, MA). The 10K MWCO dialysis membrane was purchased from Spectrum Laboratories (Rancho Dominquez, CA). Sensor chips SA and HBS−EP (pH 7.4) buffer for SPR measurements were purchased from GE Healthcare (Piscataway, NJ).

Synthesis of Oligo-Functionalized G5 PAMAM Dendrimers. The purchased G5 PAMAM dendrimer was purified with 10K MWCO dialysis, as previously described, to remove lower molecular weight impurities.[14,17] The purified G5 PAMAM dendrimer (G5-NH_2) was then chemically modified for reducing nonspecific electrostatic interactions or providing functional groups in subsequent coupling reaction of ligands (Scheme 1). Briefly, the purified amine-terminated G5 PAMAM dendrimers (200.01 mg, 7.41 μmol) were reacted with 85 equiv of acetic anhydride (59.43 μL, 629.85 μmol), which was slowly added to amine-terminated dendrimers in anhydrous MeOH (20 mL) in the presence of triethylamine (105.43 μL, 755.82 μmol) for 16 h at room temperature. The excessive solvent and reagents in the reaction were removed by rotary evaporation, followed by 10K MWCO dialysis against PBS and deionized water (DIW), respectively, for 3 cycles. The recovered partially acetylated dendrimer (G5-Ac-NH_2) was lyophilized for 3 d to yield a white solid (193.40 mg, 87%). The G5-Ac-NH_2 was subsequently modified to convert the residual primary amines to primary carboxylic groups, using glutaric anhydride. In brief, 50 equiv of glutaric anhydride (10.14 mg, 88.87 μmol) was added to G5-Ac-NH_2 (53.32 mg, 1.78 μmol) dissolved in anhydrous DMSO (5 mL) in the presence of triethylamine (12.40 μL, 88.87 μmol) for 16 h at room temperature. The mixture was purified with 10K MWCO centrifugal filters and dissolved in PBS and DIW for 4 cycles each. The recovered partially acetylated and carboxylated dendrimer (G5-Ac-COOH) was lyophilized for 3 d to yield a white solid (47.21 mg, 83%). The amide-coupling reaction of the ssDNA oligo to the dendrimers was slightly modified from the method previously described.[14] G5-Ac-COOH (6.1 mg, 0.19 μmol) was dissolved in DMSO (0.6 mL) and activated using coupling reagents, 1-ethyl-3-(-dimethylaminopropyl)arbodiimide hydrochloride (EDC) (1.05 mg, 5.56 μmol) and *N*-hydroxysuccinimide (NHS) (0.77 mg, 6.67 μmol), for 2 h at room temperature to form intermediate NHS-ester activated dendrimer. The mixture was evenly divided into three aliquots and then reacted with amine-terminated ssDNA oligos. A total of 20, 10, and 5 equiv of ssDNA oligos (1.28, 0.64, and 0.32 μmol), dissolved in 0.4 mL of pH 9 carbonate buffer were added into each aliquot with the NHS-ester activated dendrimer mixture and the mixtures were stirred for 16 h at room temperature. The mixture of the coupling reaction was purified using 10K MWCO centrifugal filters in PBS and DIW for 4 cycles each. The recovered dendrimer−ssDNA conjugates were lyophilized for 3 days to yield a white solid with yield ~80% (wt).

Characterization of Oligo-Functionalized G5 PAMAM Dendrimers. The mean number of primary amines of original and partially acetylated G5 PAMAM (G5-NH_2 and G5-Ac-NH_2) was determined by potentiometric titration using a Mettler Toledo (MP) meter and an inLab Micro electrode at room temperature as previously described.[17] Briefly, 10 mg of dendrimer was dissolved in 1 mL of 0.1 N NaCl solution. After adjustment to pH 2.5, the dendrimer solution was titrated with 0.1 N NaOH and the number of primary amines was determined by the titration curve of basification. The molecular weight of G5 PAMAM dendrimer-based ssDNA oligo nanoparticles was determined by MALDI−TOFMS using a Micromass TofSpec-2E with positive ion mode as previous described.[16] The number of attached ssDNA oligonucleotides was determined by UV−vis spectra analysis that was performed using a 1 mL quartz cuvette with a PerkinElmer Lamda 20 spectrophotometer. The equivalent concentration of ssDNA was calibrated using OD_{260} of the specific DNA sequence. The mean number of conjugated ssDNA oligo per G5 PAMAM dendrimer was determined by using the quotient of an equivalent concentration of ssDNA that the oligonucleotide-functionalized dendrimer presented and the concentration of the nanoparticles that was calculated based on the MS-determined molecular weight of the functionalized nanoparticles.

SPR Measurements. SPR experiments were conducted using a BIAcore X (Pharmacia Biosensor AB, Uppsala, Sweden), equipped with sensor chip SA, which was precoated with streptavidin on the surface, for the capture of biotinylated ssDNA oligos. Before the immobilization process, the SA surface was preconditioned with exposure to three 1 min injections containing 50 mM NaOH. The 25-mer biotinylated ssDNA oligo solution (1 mg/mL) in HBS-EP buffer was then injected only into flow channel 1 for 10 min, resulting in 1300 RU (1.3 ng/mm^2) of immobilized ssDNA oligos. After the capturing process, a 1 min injection of 10 mM NaOH was used to reduce the nonspecific binding that occurred during prior injections. A control flow channel without immobilization of 25-mer oligonucleotides was used as a reference.

During SPR measurement, the 8-mer ssDNA oligo and the oligo-functionalized dendrimer dissolved in HBS-EP buffer were injected into both flow channels of the sensor chip, including the ssDNA oligo-immobilized channel and the reference channel, at a flow rate of 10 μL/min. After each measurement, the chip surface was regenerated using 5 μL injections of pH 2 HCl-glycine buffer or 5−10 μL of pH 11 NaOH for the sample of 8-mer ssDNA oligo or the G5 ssDNA oligo-functionalized nanoparticles, respectively, to ensure complete removal of bound molecules before the next measurement. The final SPR sensograms were obtained by using the measurement after subtraction of the signal on the reference channel from the signal on the oligo-immobilized channel. After this process of referencing, the kinetic parameters, including k_{on}, k_{off}, and K_D, of the free ssDNA oligo were determined using the

Langmuir 1:1 kinetic model with default setting in BIAevaluation software.

Simulation of Distributed Valence on Nanoparticles. The statistical model assumed that ligand conjugation with the nanoparticle obeys the Poissonian stochastic mechanism. In this Poisson simulation, the total number of available attached sites on the dendrimer surface and the mean ligand number per dendrimer characterized with UV−vis and MALDI-MS were used as factors to calculate the distribution. With this method, the ligand distribution was plotted, and the percentage of nanoparticles with specific valences was identified.

Conflict of Interest: The authors declare no competing financial interest.

Supporting Information Available: Experimental details, including potentiometric titration, UV−vis spectra, MALDI−TOF mass spectrometry, and additional figures from SPR spectroscopy. This material is available free of charge *via* the Internet at http://pubs.acs.org.

Acknowledgment. This work was supported by the National Science Foundation (NSF) under Grant EFRI-BSBA 0938019. We also greatly thank support from Michigan Nanotechnology Institute for Medicine and Biological Sciences. We would also like to acknowledge Paul Trombley for his help with the abstract figure.

REFERENCES AND NOTES

1. Mammen, M.; Choi, S. K.; Whitesides, G. M. Polyvalent Interactions in Biological Systems: Implications for Design and Use of Multivalent Ligands and Inhibitors. *Angew. Chem., Int. Ed.* **1998**, *37*, 2755–2794.
2. Pieters, R. J. Maximising Multivalency Effects in Protein-Carbohydrate Interactions. *Org. Biomol. Chem.* **2009**, *7*, 2013–2025.
3. Levine, P. M.; Carberry, T. P.; Holub, J. M.; Kirshenbaum, K. Crafting Precise Multivalent Architectures. *MedChemComm* **2013**, *4*, 493–509.
4. Schrama, D.; Reisfeld, R. A.; Becker, J. C. Antibody Targeted Drugs as Cancer Therapeutics. *Nat. Rev. Drug Discovery* **2006**, *5*, 147–159.
5. Bergstrom, M.; Liu, S.; Kiick, K. L.; Ohlson, S. Cholera Toxin Inhibitors Studied with High-Performance Liquid Affinity Chromatography: A Robust Method to Evaluate Receptor-Ligand Interactions. *Chem. Biol. Drug Des.* **2009**, *73*, 132–141.
6. Toner, C. D.; Davis, C. D.; Milner, J. A. The Vitamin D and Cancer Conundrum: Aiming at a Moving Target. *J. Am. Diet. Assoc.* **2010**, *110*, 1492–1500.
7. Shen, Z.; Wei, W.; Tanaka, H.; Kohama, K.; Ma, G.; Dobashi, T.; Maki, Y.; Wang, H.; Bi, J.; Dai, S. A Galactosamine-Mediated Drug Delivery Carrier for Targeted Liver Cancer Therapy. *Pharmacol. Res.* **2011**, *64*, 410–419.
8. Sanchez-Navarro, M.; Rojo, J. Targeting Dc-Sign with Carbohydrate Multivalent Systems. *Drug News Perspect.* **2010**, *23*, 557–572.
9. Ono, M.; Kuwano, M. Molecular Mechanisms of Epidermal Growth Factor Receptor (EGFR) Activation and Response to Gefitinib and Other EGFR-Targeting Drugs. *Clin. Cancer Res.* **2006**, *12*, 7242–7251.
10. Noolvi, M. N.; Patel, H. M. Small Molecule Tyrosine Kinase Inhibitors: The New Dawn for Cancer Therapy. *Lett. Drug Des. Discovery* **2012**, *9*, 84–125.
11. Kamaly, N.; Xiao, Z.; Valencia, P. M.; Radovic-Moreno, A. F.; Farokhzad, O. C. Targeted Polymeric Therapeutic Nanoparticles: Design, Development and Clinical Translation. *Chem. Soc. Rev.* **2012**, *41*, 2971–3010.
12. Yu, M. K.; Park, J.; Jon, S. Targeting Strategies for Multifunctional Nanoparticles in Cancer Imaging and Therapy. *Theranostics* **2012**, *2*, 3–44.
13. Rizzo, L. Y.; Theek, B.; Storm, G.; Kiessling, F.; Lammers, T. Recent Progress in Nanomedicine: Therapeutic, Diagnostic and Theranostic Applications. *Curr. Opin. Biotechnol.* **2013**, *24*, 1159–1166.
14. Li, M. H.; Choi, S. K.; Thomas, T. P.; Desai, A.; Lee, K. H.; Kotlyar, A.; Banaszak Holl, M. M.; Baker, J. R., Jr. Dendrimer-Based Multivalent Methotrexates as Dual Acting Nanoconjugates for Cancer Cell Targeting. *Eur. J. Med. Chem.* **2012**, *47*, 560–572.
15. Zhang, Y. H.; Thomas, T. P.; Lee, K. H.; Li, M. H.; Zong, H.; Desai, A. M.; Kotlyar, A.; Huang, B. H.; Holl, M. M. B.; Baker, J. R. Polyvalent Saccharide-Functionalized Generation 3 Poly(amidoamine) Dendrimer-Methotrexate Conjugate as a Potential Anticancer Agent. *Bioorg. Med. Chem.* **2011**, *19*, 2557–2564.
16. Zong, H.; Thomas, T. P.; Lee, K. H.; Desai, A. M.; Li, M. H.; Kotlyar, A.; Zhang, Y. H.; Leroueil, P. R.; Gam, J. J.; Holl, M. M. B.; Baker, J. R., Jr. Bifunctional PAMAM Dendrimer Conjugates of Folic Acid and Methotrexate with Defined Ratio. *Biomacromolecules* **2012**, *13*, 982–991.
17. Mullen, D. G.; Fang, M.; Desai, A.; Baker, J. R.; Orr, B. G.; Holl, M. M. B. A Quantitative Assessment of Nanoparticle-Ligand Distributions: Implications for Targeted Drug and Imaging Delivery in Dendrimer Conjugates. *ACS Nano* **2010**, *4*, 657–670.
18. Mullen, D. G.; Borgmeier, E. L.; Desai, A. M.; van Dongen, M. A.; Barash, M.; Cheng, X. M.; Baker, J. R.; Holl, M. M. B. Isolation and Characterization of Dendrimers with Precise Numbers of Functional Groups. *Chem.—Eur. J.* **2010**, *16*, 10675–10678.
19. Persson, B.; Stenhag, K.; Nilsson, P.; Larsson, A.; Uhlen, M.; Nygren, P. A. Analysis of Oligonucleotide Probe Affinities Using Surface Plasmon Resonance: A Means for Mutational Scanning. *Anal. Biochem.* **1997**, *246*, 34–44.
20. Nishikawa, M.; Rattanakiat, S.; Takakura, Y. DNA-Based Nano-Sized Systems for Pharmaceutical and Biomedical Applications. *Adv. Drug Delivery Rev.* **2010**, *62*, 626–632.
21. Bandy, T. J.; Brewer, A.; Burns, J. R.; Marth, G.; Nguyen, T.; Stulz, E. DNA as Supramolecular Scaffold for Functional Molecules: Progress in DNA Nanotechnology. *Chem. Soc. Rev.* **2011**, *40*, 138–148.
22. Hong, S.; Leroueil, P. R.; Majoros, I. J.; Orr, B. G.; Baker, J. R., Jr.; Banaszak Holl, M. M. The Binding Avidity of a Nanoparticle-Based Multivalent Targeted Drug Delivery Platform. *Chem. Biol.* **2007**, *14*, 107–115.
23. Tassa, C.; Duffner, J. L.; Lewis, T. A.; Weissleder, R.; Schreiber, S. L.; Koehler, A. N.; Shaw, S. Y. Binding Affinity and Kinetic Analysis of Targeted Small Molecule-Modified Nanoparticles. *Bioconjugate Chem.* **2010**, *21*, 14–19.
24. Svenson, S.; Tomalia, D. A. Dendrimers in Biomedical Applications—Reflections on the Field. *Adv. Drug Delivery Rev.* **2005**, *57*, 2106–2129.
25. Menjoge, A. R.; Kannan, R. M.; Tomalia, D. A. Dendrimer-Based Drug and Imaging Conjugates: Design Considerations for Nanomedical Applications. *Drug Discovery Today* **2010**, *15*, 171–185.
26. Edwards, P. R.; Leatherbarrow, R. J. Determination of Association Rate Constants by an Optical Biosensor Using Initial Rate Analysis. *Anal. Biochem.* **1997**, *246*, 1–6.
27. Thomas, T. P.; Huang, B.; Choi, S. K.; Silpe, J. E.; Kotlyar, A.; Desai, A. M.; Zong, H.; Gam, J.; Joice, M.; Baker, J. R., Jr. Polyvalent Dendrimer-Methotrexate as a Folate Receptor-Targeted Cancer Therapeutic. *Mol. Pharmaceutics* **2012**, *9*, 2669–2676.
28. Choi, S. K.; Myc, A.; Silpe, J. E.; Sumit, M.; Wong, P. T.; McCarthy, K.; Desai, A. M.; Thomas, T. P.; Kotlyar, A.; Holl, M. M.; Orr, B. G.; Baker, J. R., Jr. Dendrimer-Based Multivalent Vancomycin Nanoplatform for Targeting the Drug-Resistant Bacterial Surface. *ACS Nano* **2013**, *7*, 214–228.
29. Silpe, J. E.; Sumit, M.; Thomas, T. P.; Huang, B.; Kotlyar, A.; van Dongen, M. A.; Banaszak Holl, M. M.; Orr, B. G.; Choi, S. K. Avidity Modulation of Folate-Targeted Multivalent Dendrimers for Evaluating Biophysical Models of Cancer Targeting Nanoparticles. *ACS Chem. Biol.* **2013**, *8*, 2063–2071.